Research Square

Preprints are preliminary reports that have not undergone peer review.
They should not be considered conclusive, used to inform clinical practice,
or referenced by the media as validated information.

Hypoxia-driven HIF1A-HK2-dependent glycolytic reprogramming contributes to sorafenib tolerance in hepatocellular carcinoma

Haijun Chen
Jinhua Central Hospital
Lujian Zhu
Jinhua Central Hospital
Junmei Lin
Jinhua Central Hospital
Xuxing Ye
Jinhua Central Hospital
Hongjun Hua
Jinhua Central Hospital
Chao Yang
Hangzhou First People's Hospital
Xiaobo Wang
wxb19920506@163.com

Jinhua Central Hospital

Research Article

Keywords: Hepatocellular carcinoma, Hypoxia, HK2, Glycolytic reprogramming, Sorafenib resistance

Posted Date: March 19th, 2026

DOI: https://doi.org/10.21203/rs.3.rs-8732871/v1

License: This work is licensed under a Creative Commons Attribution 4.0 International License.
Read Full License

Additional Declarations: No competing interests reported.

Abstract

Background

Hepatocellular carcinoma (HCC) is characterized by pronounced hypoxia and suboptimal response to sorafenib, but how hypoxia in defined malignant cell subsets drives metabolic adaptation and drug tolerance remains unclear. This study aimed to identify hypoxia-dominant tumor populations, derive a hypoxia-related risk signature, and determine whether a HIF1A-HK2 axis mediates glycolytic reprogramming and sorafenib resistance through tumor cell-intrinsic mechanisms.

Methods

Single-cell RNA sequencing from ten HCC samples was integrated with bulk transcriptomic cohorts to define a hypoxia-enriched epithelial subcluster, construct a seven-gene hypoxia-related risk model, and screen for a stable metabolic node, followed by hypoxia modelling (1% O_2/$CoCl_2$), HK2 knockdown/overexpression, co-immunoprecipitation, promoter-focused structural modelling, and functional assays of glycolysis, sorafenib sensitivity and endothelial tube formation.

Results

The analysis identified a hypoxia-high malignant subcluster whose gene set generated a seven-gene signature that stratified survival and reflected activation of hypoxia and glycolysis pathways; HK2 was consistently retained across subcluster screening, risk modelling and pathway annotation, and in vitro HIF1A stabilization increased HK2 expression, glycolytic flux and sorafenib survival, while HK2 knockdown reduced glycolysis and partially restored sorafenib sensitivity and HK2 overexpression in normoxia reproduced a hypoxia-like metabolic and drug-response profile without major effects on endothelial tube formation.

Conclusions

These findings indicate that a hypoxia-associated HIF1A-HK2 axis acts as a tumor cell-intrinsic driver of glycolytic support for sorafenib tolerance and suggest that hypoxia- and glycolysis-related features may refine risk stratification and inform metabolic co-targeting strategies in HCC.

Introduction

Hepatocellular carcinoma (HCC) represents one of the most lethal malignancies worldwide, with rising incidence and persistently poor survival despite therapeutic progress(Bray et al. 2024). For patients with advanced-stage disease, systemic therapies remain the mainstay of treatment, and sorafenib has served as a foundational first-line agent for more than a decade(Sangro et al. 2025). Nevertheless, intrinsic and

acquired resistance markedly constrain its clinical benefit, underscoring the urgent need to delineate the biological programs that enable tumor survival under treatment pressure(Tang et al. 2020).

A defining feature of the HCC microenvironment is hypoxia, arising from abnormal vasculature, rapid tumor expansion and elevated metabolic demand(Bao and Wong 2021). Hypoxia stabilizes hypoxia-inducible factor 1α (HIF1A), which coordinates extensive transcriptional remodeling and drives metabolic and phenotypic adaptation(Liu et al. 2024; Semenza 2002). Through this process, hypoxic tumors often exhibit heightened glycolytic dependence, immune-suppressive remodeling and increased therapeutic tolerance(Ladd et al. 2024). However, the extent to which distinct hypoxia-dominant malignant subsets exist within HCC—and how these subpopulations link hypoxic signaling to clinically relevant drug resistance—remains insufficiently characterized(An and Li 2025).

Advances in single-cell transcriptomics now enable precise dissection of intratumoral heterogeneity and reveal malignant populations that may be obscured in bulk analyses(Zhan et al. 2025). Yet, most hypoxia-related studies in HCC rely on bulk measurements, making it impossible to pinpoint the specific cell states that carry hypoxic programs or determine whether such states predict prognosis and treatment response(Jiang et al. 2021; Zeng et al. 2021; Zhang et al. 2021). Moreover, although hypoxia is widely associated with metabolic reprogramming and sorafenib resistance, the mechanistic path connecting hypoxic transcriptional states, metabolic adaptations and therapeutic tolerance is not fully resolved(Tang et al. 2018). It remains unclear whether a discrete malignant subpopulation defined by hypoxia exists, whether such a population can generate a prognostically meaningful molecular signature, and whether this signature converges on specific metabolic regulators that shape sorafenib sensitivity(Jin et al. 2022; Yang et al. 2025). Additionally, whether hypoxia-associated resistance is dependent on angiogenic remodeling or arises through tumor cell-intrinsic pathways remain to be determined.

In this study, we address these gaps using a multi-layered strategy that integrates single-cell transcriptomic profiling, prognostic modeling, multiomic correlation analyses and functional validation. We first identify, at single-cell resolution, a malignant epithelial subpopulation with dominant hypoxic activity and then derive a hypoxia-related seven-gene model that robustly stratifies patient survival. This model highlights a key metabolic node emerging from the hypoxic subcluster, which we subsequently investigate through biochemical assays, hypoxia-mimetic stimulation, genetic perturbation and sorafenib response testing. To define the regulatory architecture, we combine protein-protein and protein-DNA interaction analyses with structural modeling. Finally, to distinguish tumor cell-intrinsic mechanisms from angiogenic effects, we evaluate endothelial tube formation in the context of metabolic perturbation.

Collectively, this work provides an integrated framework that links hypoxia-defined malignant cell states to metabolic adaptation and sorafenib resistance, and establishes a mechanistic chain that connects transcriptional programs, regulatory interactions and functional outcomes. These findings refine the

understanding of hypoxia-driven heterogeneity in HCC and suggest potential avenues for improving therapeutic strategies.

Materials and Methods

Data acquisition and preprocessing

Publicly available single-cell RNA sequencing (scRNA-seq) datasets comprising ten primary HCC samples with comprehensive clinical annotations were retrieved from GSE149614(Lu et al. 2022). Raw count matrices were processed using the Seurat package (version 5.4) in R(Satija et al. 2015). Stringent quality control was applied to filter low-quality cells based on the following metrics: (i) fewer than 200 detected genes, (ii) more than 5,000 detected genes, or (iii) mitochondrial gene proportion exceeding 15%. Genes expressed in fewer than three cells were excluded. Counts were normalized using a log-normalization procedure and scaled to 10,000 transcripts per cell. Data normalization was performed using the global-scaling log-normalization method, followed by scaling to 10,000 transcripts per cell. To mitigate batch effects, canonical correlation analysis (CCA) and integration anchors were employed. Dimensionality reduction was subsequently performed using Principal Component Analysis (PCA), and cellular landscapes were visualized via Uniform Manifold Approximation and Projection (UMAP).

For bulk RNA-seq and clinical data, the TCGA-LIHC cohort and independent validation sets were downloaded from the corresponding portals. Expression data were converted to transcripts per million (TPM) and log2-transformed. Patients with missing survival information or overall survival < 30 days were excluded from prognostic modelling.

Single-cell Annotation and Hypoxia Scoring

Following integration, a shared nearest neighbor (SNN) graph was constructed using significant principal components, and unsupervised clustering was performed via the Louvain algorithm at an empirically optimized resolution. Major cell lineages were annotated by canonical markers: epithelial/tumor cells, fibroblasts, endothelial cells, myeloid cells, T/NK cells, B/plasma cells and mast cells. Marker expression was displayed using dot plots and feature plots.

The epithelial subpopulation was isolated and re-clustered to identify distinct malignant states (C0-C5). To quantify hypoxic activity, Gene Set Variation Analysis (GSVA) was applied using a predefined hypoxia hallmark gene set. Malignant clusters exhibiting significantly elevated hypoxia scores were designated as "hypoxia-dominant" subpopulations and utilized for downstream signature derivation(Hänzelmann et al. 2013).

Construction of the hypoxia-related risk model

Genes significantly enriched in the hypoxia-dominant cluster (adjusted $P < 0.05$, |log2FC| > 0.5) were intersected with the TCGA-LIHC bulk dataset. Prognostic candidates were initially screened using univariate Cox proportional hazards regression. A Least Absolute Shrinkage and Selection Operator (LASSO) Cox regression model was subsequently established to minimize overfitting, with the optimal penalty parameter (λ) determined via 10-fold cross-validation. The risk score was calculated as: Risk Score = $\sum (Expression_i \times Coefficient_i)$. Patients were stratified into high- and low-risk groups based on the median risk score. Survival differences were assessed using Kaplan-Meier analysis with the log-rank test, and predictive accuracy was evaluated using time-dependent Receiver Operating Characteristic (ROC) curves.

Functional Enrichment and Immune Landscape Analysis

Differentially expressed genes (DEGs) between risk groups were identified using the limma package (adjusted $P < 0.05$, |log2FC| > 1)(Ritchie et al. 2015). Gene Set Enrichment Analysis (GSEA) was conducted to elucidate biological functions, focusing on hypoxia, HIF-1 signaling, and glycolysis pathways. Pathway activities were further quantified using GSVA and Single-Sample GSEA (ssGSEA). Spearman's correlation analysis was performed to evaluate the associations among *HK2*, *HIF1A*, hypoxia scores, and glycolysis signatures.

The immune landscape was deconvoluted using CIBERSORT to estimate the abundance of tumor-infiltrating immune cells(Newman et al. 2015). Intercellular communication between the hypoxia-dominant malignant cluster and immune subsets was inferred using CellChat, visualizing ligand-receptor interactions via circos and dot plots(Jin et al. 2021).

Drug sensitivity prediction

Chemotherapeutic response was predicted using the oncoPredict algorithm(Maeser et al. 2021). Ridge regression was employed to estimate the half-maximal inhibitory concentration (IC_{50}) of sorafenib and other targeted agents based on transcriptomic profiles. Differences in predicted drug sensitivity between risk groups were analyzed statistically.

Cell Culture and Hypoxia Modeling

Human HCC cell lines (Huh7, Hep3B) and human umbilical vein endothelial cells (HUVECs) were obtained from Cell Resource Center, Peking Union Medical College (Beijing, China) and authenticated via Short Tandem Repeat (STR) profiling. Cells were cultured in DMEM or endothelial growth medium supplemented with 10% fetal bovine serum (FBS) and antibiotics at 37°C in a 5% CO_2 incubator. All lines were confirmed to be mycoplasma-free.

Hypoxic conditions were simulated using two distinct methods: (i) Physical Hypoxia: Incubation in a hypoxia chamber (1% O_2, 5% CO_2, 94% N_2); and (ii) Chemical Hypoxia: Treatment with Cobalt Chloride ($CoCl_2$, 100 μM) to stabilize HIF1A(Caltana et al. 2009). Normoxic controls were maintained at 21% O_2.

Genetic Manipulation and Sorafenib Treatment

Transient knockdown of HK2 was achieved using specific small interfering RNAs (siRNAs), with non-targeting siRNA serving as a control. Overexpression was performed using a full-length human HK2 cDNA vector. Transfections were carried out using Lipofectamine 3000 following the manufacturer's protocol. Transfection efficiency was validated by Western blotting 48–72 h post-transfection.

For drug assays, sorafenib (Cat. No. HY-10201; MedChemExpress) was dissolved in DMSO. Cells pre-exposed to normoxic or hypoxic conditions were treated with sorafenib at indicated concentrations. Controls received an equivalent volume of DMSO.

Western Blotting and Co-Immunoprecipitation (Co-IP)

Total protein was extracted using RIPA lysis buffer containing protease/phosphatase inhibitors. Lysates were quantified via BCA assay, resolved by SDS-PAGE, and transferred to PVDF membranes. Blots were probed with primary antibodies against HIF1A (Cat. No. ab179483; Abcam), HK2 (Cat. No. ab209847; Abcam), and GAPDH (Cat. No. ab181602; Abcam), followed by HRP-conjugated secondary antibodies. Bands were visualized using Enhanced Chemiluminescence (ECL) and quantified via ImageJ software.

For Co-IP, lysates were incubated with anti-HIF1A, anti-HK2, or control IgG antibodies at 4°C overnight, followed by capture with Protein A/G agarose beads. Immunocomplexes were washed, eluted, and analyzed by Western blotting to assess protein-protein interactions under normoxic and hypoxic conditions.

Structural modelling of HIF1A-HK2 promoter interaction

The interaction between the HIF1A DNA-binding domain and the HK2 promoter containing the Hypoxia Response Element (HRE) was modeled using AlphaFold3(Peng et al. 2025). Sequence data were retrieved from UniProt. The predicted structural models were visualized and analyzed using PyMOL, focusing on hydrogen bonding and steric compatibility at the binding interface.

Metabolic Assays

Glycolytic Flux: The Extracellular Acidification Rate (ECAR) was measured using a Seahorse XF Analyzer (Agilent). Cells were subjected to a Glycolysis Stress Test involving sequential injections of glucose, oligomycin, and 2-deoxy-D-glucose (2-DG) per standard protocols.

Lactate and Glucose Uptake: Lactate concentrations in conditioned media were quantified using a colorimetric/fluorometric kit (Cat. No. ab65330; Abcam). Glucose uptake was assessed by measuring the intracellular accumulation of labeled 2-DG. Data were normalized to total cell number or protein concentration.

Cell Viability and Tube Formation Assays

Cell viability was determined using the Cell Counting Kit-8 (CCK-8). Post-treatment, cells were incubated with CCK-8 reagent for 1–2 h, and absorbance was measured at 450 nm. For angiogenesis assays, HUVECs were seeded on Matrigel-coated plates (Corning) and treated with conditioned media from HCC cells. After 4–8 h, capillary-like tube formation was imaged using an inverted microscope. Total tube length and junction number were quantified using the Angiogenesis Analyzer plugin in ImageJ.

Statistical analysis

Data are presented as mean ± standard deviation (SD) or median (interquartile range). Statistical comparisons were performed using Student's *t*-test, Mann-Whitney *U* test, one-way ANOVA, or Kruskal-Wallis test, as appropriate. Survival analysis utilized the Kaplan-Meier method and log-rank tests. Correlations were assessed using Pearson or Spearman coefficients. Analyses were conducted using R (v4.4.2) and GraphPad Prism (v9.5). A two-sided $P < 0.05$ was considered statistically significant.

Results

Single-cell transcriptomic profiling and cell-type annotation of HCC samples

We first integrated single-cell RNA-seq data from 10 HCC samples (HCC01T-HCC10T) and performed batch correction. As shown in Fig. 1A, cells from different samples were well mixed in the UMAP plot, indicating effective removal of batch effects. We then performed unsupervised clustering to classify all cells into major cell types (Fig. 1B). Based on canonical marker genes (Fig. 1C), we annotated the clusters as follows: epithelial cells (high expression of CLDN5, CRHBP, SPINK1), fibroblasts (ACTA2, DCN, MGP), endothelial cells (HP, TFF2, TPSAB1), T cells (CD3D, CD3E, CD8A), NK cells (GZMB, CCL4, KLRCl), B cells (IGHG1, IGHG4, JCHAIN), plasma cells (IGHG1, IGHG4, JCHAIN), mast cells (TPSB2, CPA3, S100A9), and myeloid cells (CD68, CD163). This annotation provided a comprehensive overview of the cellular composition within the HCC tumor microenvironment.

To further investigate tumor cell heterogeneity, we extracted epithelial cells for downstream analysis. The integrated UMAP visualization of tumor cells from the 10 samples showed well-mixed distributions (Fig. 1D). Unsupervised clustering identified six distinct tumor cell subpopulations, designated C0-C5 (Fig. 1E). Each subpopulation exhibited unique transcriptional profiles, suggesting functional heterogeneity. GSVA revealed that C2 displayed the highest hypoxia score among all subpopulations (Fig. 1F), implying that this cluster likely resides in the hypoxic tumor core. These findings indicate that

the C2 subpopulation may play a central role in hypoxia-driven tumor progression, warranting further detailed investigation.

Hypoxia-associated seven-gene model identifies high-risk subsets and highlights HK2 as a metabolic vulnerability in HCC

To identify prognostic determinants arising from the hypoxia-enriched malignant epithelial subpopulation identified previously, we constructed a hypoxia-related survival model using LASSO-Cox regression. As the regularization strength increased, the majority of hypoxia-responsive genes were progressively compressed toward zero, leaving only a stable subset with retained coefficients (Fig. 2A), and ten-fold cross-validation determined the optimal λ minimizing prediction error (Fig. 2B). This refinement produced a seven-gene signature capable of stratifying TCGA-LIHC patients into high- and low-risk groups, in which Kaplan-Meier analysis revealed significantly longer survival for the low-risk group ($p < 0.0001$; Fig. 2C), consistent with the distribution of calculated scores (Fig. 2D) and the accumulation of death events in the high-risk cohort (Fig. 2E).

To understand the biological underpinnings of this risk divergence, we compared transcriptomic differences between the two groups and observed enriched expression of prognosis-associated genes in the high-risk state (Fig. 2F). Notably, among the retained components, HK2 emerged as a leading contributor, consistent with its selective elevation within the C2 hypoxia-dominant subcluster identified in our single-cell analysis. Pathway enrichment further demonstrated that high-risk tumors were driven by hypoxia-dependent oncogenic programs, including the HIF-1 and VEGF signaling pathways (Fig. 2G-H), highlighting a metabolic-angiogenic adaptation axis. Supporting this mechanism, high-risk tumors exhibited stronger hypoxia and glycolysis activation (Fig. 2I), and HK2 expression correlated positively with hypoxia score, HIF1A levels, and glycolytic flux (Fig. 2J-L), positioning HK2 as a metabolic node linking hypoxia signaling to tumor aggressiveness and providing rationale for downstream functional interrogation.

Hypoxia-high tumors exhibit immune-suppressive remodeling driven by HK2-linked malignant C2 signals

To determine whether hypoxia-HK2 activity was linked to immunological remodeling, we profiled immune cell distribution across risk states. Immune-correlation matrices showed coordinated enrichment among suppressive subsets including M2 macrophages, Tregs and mast cells, while cytotoxic NK and effector $CD8^+$ T cells exhibited weaker coupling (Fig. 3A). Consistently, high-risk tumors displayed increased infiltration of M2 macrophages and Tregs accompanied by reduced naïve T-cell signatures compared with the low-risk group (Fig. 3B), suggesting that HK2-high hypoxic tumors may promote an immune-evasive microenvironment. Correlation heatmaps further demonstrated that HK2 expression positively associated with hypoxia-linked mitochondrial regulators HIGD2A, EPO, HILPDA and HIGD1C, whereas tumor suppressor signals such as TP53 were negatively correlated (Fig. 3C-D), reinforcing HK2 as a

metabolic hub under hypoxic pressure. Ligand-receptor inference revealed that malignant C2 cells preferentially communicated with macrophages and T cells through MDK, ANGPTL4, PPIA, SDC2 and BSG signaling axes (Fig. 3E), and probability ranking highlighted SPP1-CD44, PROS1-MERTK, MIF-(CD74 + CXCR4/CD44) and MDK-SDC2/NCL as dominant outgoing interactions shaping immune polarization (Fig. 3F). Together, these findings indicate that hypoxia-driven HK2 activity not only enhances metabolic adaptation but also conveys immunomodulatory signals that reinforce M2 dominance and T-cell dysfunction, supporting an immune-suppressive tumor ecosystem.

Hypoxic stimulation stabilizes HIF1A, induces HK2 expression and confers a sorafenib survival advantage

Based on the above genomic and microenvironmental evidence, we next sought to validate the HIF1A-HK2 axis at the protein level and determine its impact on sorafenib response. We established two complementary hypoxia models in Huh7 and Hep3B cells using 1% O_2 and $CoCl_2$ treatment. Western blotting showed that both physical and chemical hypoxia robustly increased HIF1A protein abundance, accompanied by a marked elevation of HK2 in both cell lines compared with normoxic controls (Fig. 4A-H). These results confirmed that HK2 is a hypoxia-inducible effector downstream of HIF1A in HCC cells.

To connect hypoxia-driven HK2 induction with therapeutic response, we next assessed the sensitivity of high- and low-risk tumors to multiple targeted agents. Drug-response analysis at the transcriptomic level revealed broader IC_{50} distributions in the high-risk group, with sorafenib displaying the most pronounced resistance pattern among the evaluated compounds (Fig. 4I). Consistent with the in-silico prediction, CCK-8 assays showed that both 1% O_2 and $CoCl_2$ significantly increased cell viability across a range of sorafenib concentrations in Huh7 and Hep3B cells, resulting in a rightward shift of the dose-response curves relative to normoxia (Fig. 4J-K). Together with the risk-model analyses, these data establish a functional link between hypoxia-induced HIF1A-HK2 activation and sorafenib tolerance in HCC.

HIF1A directly associates with HK2 and binds the HK2 promoter through an HRE-containing region

To elucidate whether HK2 is directly controlled by HIF1A at the transcriptional level, we first examined the physical interaction between the two proteins. Co-immunoprecipitation experiments performed in Huh7 and Hep3B under normoxia, 1% O_2 and $CoCl_2$ conditions showed reciprocal pull-down of HIF1A and HK2, indicating the presence of a protein complex between HIF1A and HK2 under both basal and hypoxic states (Fig. 5A-D).

We then explored the structural basis of transcriptional regulation by focusing on the HK2 promoter. Using UniProt-derived sequences, we selected a promoter fragment containing a canonical HRE and submitted this DNA segment to AlphaFold3 for protein-DNA complex modeling in combination with the HIF1A DNA-binding domain. The resulting structural model showed HIF1A docked into the major groove of the HK2 promoter, with the HRE region clearly positioned at the interface (Fig. 5E). Hydrogen-bond analysis in PyMOL revealed multiple contacts between the HRE bases and key residues within the HIF1A

DNA-binding domain, supporting a direct transcriptional control mechanism. These findings, together with the co-IP data, establish that HIF1A not only forms a complex with HK2 but also directly engages the HK2 promoter through an HRE-containing element to drive its transcription under hypoxia.

HK2 knockdown suppresses glycolytic flux and reverses hypoxia-induced sorafenib resistance, whereas HK2 overexpression reproduces a hypoxia-like phenotype

To functionally dissect the role of HK2 in hypoxia-driven metabolic reprogramming and drug resistance, we generated both loss-of-function and gain-of-function models in Huh7 and Hep3B cells. siRNA-mediated knockdown using siHK2-3 markedly reduced HK2 protein levels in both cell lines, whereas ectopic expression of HK2 produced a robust overexpression phenotype (Fig. 6A-F). These complementary models allowed us to directly quantify the contribution of HK2 to glycolytic metabolism and drug response under defined oxygen conditions.

Seahorse ECAR assays demonstrated that HK2 knockdown significantly decreased glycolytic flux in Huh7 and Hep3B cells cultured under 1% O_2 or $CoCl_2$, while HK2 overexpression enhanced ECAR even in the absence of hypoxia (Fig. 6G-L). Consistent with the real-time flux measurements, biochemical assays showed that lactate production and glucose uptake were both diminished upon HK2 silencing and increased in HK2-overexpressing cells, with the greatest differences observed under hypoxic stimulation (Fig. 6G-L). These results indicate that HK2 is not merely a downstream marker of hypoxia but a rate-limiting effector that determines the magnitude of glycolytic throughput. In other words, the presence or absence of HK2 directly sets the “ceiling” of glycolytic capacity, which aligns with its central position in the hypoxia-associated risk model derived from patient cohorts.

We next examined whether these HK2-dependent metabolic changes translated into altered sorafenib sensitivity. At a fixed sorafenib concentration approximating clinically relevant exposure, HK2 knockdown markedly reduced cell viability under both 1% O_2 and $CoCl_2$, partially restoring the cytotoxic effect of sorafenib compared with HK2-NC controls (Fig. 6M-N). In contrast, HK2 overexpression increased survival in sorafenib-treated cells even under normoxic conditions, thereby reproducing a hypoxia-like resistant phenotype in the absence of actual hypoxic stress (Fig. 6M-N). Integrating these findings, HK2 fulfils both criteria of a functional driver: it is necessary for maintaining glycolytic support of survival under hypoxia, and sufficient to impose a resistant metabolic state under normoxia when overexpressed. In the context of the earlier single-cell and risk-model analyses, these data establish HK2 as the key metabolic switch that converts hypoxia-associated transcriptional programs into a concrete survival advantage under sorafenib treatment.

HK2-mediated sorafenib resistance is independent of endothelial tube formation

Because hypoxia and VEGF pathway activation are classically linked to pro-angiogenic remodeling, we further assessed whether the HK2-driven survival advantage was accompanied by changes in endothelial tube formation. Conditioned medium from Huh7 and Hep3B cells transfected with HK2-NC,

siHK2-3, or ovHK2 and cultured under normoxia, 1% O_2 or $CoCl_2$ was applied to HUVECs in a Matrigel-based tube formation assay. Microscopic evaluation revealed comparable network architecture across all groups, without obvious disruption or enhancement of capillary-like structures associated with HK2 knockdown or overexpression under any oxygen condition (Fig. 7A-B). Quantitative analysis of junction numbers per field confirmed the absence of meaningful differences between conditions (Fig. 7C-D).

When interpreted together with the pronounced effects of HK2 manipulation on glycolytic activity and sorafenib response, these observations indicate a dissociation between HK2-dependent metabolic reprogramming and angiogenic behavior in this setting. In other words, the survival benefit conferred by HK2 is not mediated through altered endothelial tube-forming capacity or paracrine promotion of vascular morphogenesis, despite the enrichment of VEGF signaling at the transcriptomic level in high-risk tumors. Instead, the data support a model in which HK2 primarily acts within tumor cells to rewire intracellular energy metabolism and sustain drug tolerance, while leaving gross endothelial tube formation largely unchanged. This distinction functionally separates hypoxia-HIF1A-HK2-driven metabolic resistance from classical hypoxia-VEGF-driven angiogenic adaptation, and highlights HK2-centred glycolytic control as a tumor-intrinsic mechanism of sorafenib resistance.

Discussion

In this study, we combined single-cell transcriptomics, prognostic modeling and experimental perturbation to investigate how hypoxia-associated programs shape metabolic adaptation and sorafenib response in hepatocellular carcinoma. At the single-cell level, we identified a malignant epithelial subpopulation with the highest hypoxia score among tumor clusters and used its enriched gene set to construct a seven-gene hypoxia-related risk model. This model effectively stratified bulk HCC patients into distinct prognostic groups, in which high-risk tumors displayed stronger hypoxia and glycolytic activation. Within this analytical framework, HK2 was repeatedly retained when we moved from hypoxic subcluster definition to LASSO-based feature selection and pathway annotation, and was therefore taken forward for mechanistic validation. In vitro hypoxia models confirmed that HIF1A stabilization was accompanied by HK2 upregulation, enhanced glycolytic flux and reduced sorafenib sensitivity, while HK2 knockdown had the opposite effect. Finally, endothelial tube formation assays suggested that HK2 manipulation had little impact on capillary-like network formation, indicating that the HK2-related survival advantage under sorafenib occurs largely through tumor-intrinsic metabolic changes rather than overt pro-angiogenic remodeling.

Previous work has established hypoxia as a hallmark of HCC progression and treatment resistance, mainly based on bulk transcriptomic signatures and hypoxia scoring across cohorts(Zhang et al. 2020). However, such approaches cannot readily distinguish which malignant cell states carry these signals. By starting from single-cell data and identifying a hypoxia-dominant epithelial subset, our analysis provides a more granular view of intratumoral heterogeneity(Ho et al. 2021). The seven-gene risk model derived from this subset not only stratified overall survival but also recapitulated key hypoxia-related pathways, including HIF-1 signalling and glycolysis, in the high-risk group. These findings support the notion that

hypoxia is not uniformly distributed across malignant cells but is concentrated in specific subsets that are both transcriptionally and clinically relevant(Lin et al. 2025). In this context, linking a bulk risk score back to a defined hypoxic tumor cluster adds cellular context to existing hypoxia-based stratification schemes and may facilitate more precise interpretation of risk in future studies.

On this basis, we next focused on the metabolic component of the hypoxia-associated program. Glycolytic reprogramming is a common feature of hypoxic tumors, and members of the HK family, particularly HK2, have been implicated in lactate production and survival under stress(Li et al. 2025; Wang et al. 2022). In our workflow, HK2 was not selected a priori but emerged as the most consistent candidate when we followed the analytical pipeline: it was enriched in the hypoxic C2 subcluster, retained as a coefficient in the hypoxia risk model after LASSO shrinkage, and strongly associated with glycolysis-related signatures in pathway analyses. This stepwise narrowing provided the rationale for mechanistic experiments centred on HK2. In Huh7 and Hep3B cells, both 1% O_2 and $CoCl_2$ treatment stabilized HIF1A and increased HK2 protein levels, in line with the transcriptomic associations observed in patient datasets. Functional assays showed that HK2 knockdown reduced ECAR, lactate release and glucose uptake, particularly under hypoxic conditions, while HK2 overexpression in normoxia produced a glycolytic profile resembling that seen in hypoxia. These results suggest that HK2 acts as an important effector of hypoxia-driven glycolytic output in HCC cells, translating upstream transcriptional adaptation into measurable metabolic flux(Wang et al. 2024).

We then examined how these metabolic changes influenced sorafenib response. Clinical and experimental data have shown that hypoxic tumors tend to be less responsive to multi-kinase inhibitors, but the relative contributions of vascular versus metabolic mechanisms remain incompletely defined. In our analyses, high hypoxia risk scores were associated with broader IC_{50} distributions for several agents, with sorafenib showing the most marked shift between risk groups. Consistently, hypoxic culture conditions increased cell viability under sorafenib treatment in both cell lines. When HK2 was silenced, this hypoxia-induced survival advantage was partially reversed, whereas HK2 overexpression under normoxic conditions increased viability at a fixed sorafenib concentration. The directionality of these effects supports a functional role for HK2 in modulating drug tolerance: higher HK2 levels align with enhanced glycolysis and relative resistance, whereas reduced HK2 limits glycolytic capacity and restores sensitivity(Cao et al. 2020; Garcia et al. 2019). Although sorafenib resistance is a multifactorial process, our data indicate that HK2-mediated glycolytic adaptation represents one important component of the hypoxia-associated phenotype(Tang, Chen, Zhang, Cheng, Zhang, Wu, Wang, Wang, Rong, Reiter, De Toni and Wang 2020).

Given the classical link between hypoxia, VEGF signalling and angiogenesis in HCC(Li et al. 2022; Shan et al. 2024), we also addressed whether HK2-related changes were accompanied by altered endothelial behaviour. Conditioned medium from HCC cells with HK2 knockdown or overexpression, cultured under normoxia, 1% O_2 or $CoCl_2$, did not induce major differences in HUVEC tube formation. Quantitative analysis of junction numbers per field supported the visual impression that capillary-like structures were broadly comparable across conditions. Taken together with the clear impact of HK2 on glycolysis and

sorafenib response, these findings suggest that, in this experimental setting, the survival benefit associated with HK2 is largely independent of measurable changes in endothelial tube formation. This does not negate the importance of VEGF-driven angiogenesis in HCC, but it does highlight that hypoxia-associated resistance can be mediated through tumor cell-intrinsic metabolic pathways even when gross angiogenic readouts are unchanged(Do et al. 2023; Sun et al. 2013).

The present work carries several implications. From a biological perspective, it connects a hypoxia-enriched malignant subset at single-cell level to a clinically relevant risk model and then to a specific metabolic effector that can be experimentally perturbed. From a translational viewpoint, the data raise the possibility that patients with high hypoxia or glycolysis scores, and particularly those with elevated HK2 expression, may represent a subgroup at increased risk of sorafenib tolerance, in whom early combination with metabolic interventions could be considered in future trials. In addition, HK2 and related glycolytic markers may have value as tissue or liquid biopsy readouts for monitoring the evolution of metabolic resistance over time. These ideas remain speculative at this stage but provide a framework for subsequent clinical validation(Zhu et al. 2024).

Several limitations should be acknowledged. First, functional experiments were restricted to two HCC cell lines and in vitro conditions, which cannot fully recapitulate the complexity of the tumor microenvironment, including immune and stromal components(Yan et al. 2024). Second, sorafenib was the only systemic agent examined; whether similar HK2-dependent effects extend to other tyrosine kinase inhibitors or immunotherapies remains unclear(Wang et al. 2025). Third, our metabolic analyses focused on glycolysis, and other pathways such as glutamine metabolism, fatty acid oxidation and mitochondrial function were not systematically evaluated(Yang et al. 2021). Finally, the evidence for direct HIF1A binding to the HK2 promoter is based on structural modelling and co-immunoprecipitation; chromatin-based assays in tumor samples will be required to confirm the regulatory interface in vivo(Ferrer et al. 2014). These limitations define the boundaries of the current work and suggest directions for refinement.

Future studies may build on this framework in several ways. In vivo models incorporating hypoxia gradients, immune cells and vascular dynamics could be used to determine to what extent HK2 dependence is maintained under therapeutic pressure. Longitudinal sampling of patients receiving sorafenib or other targeted agents may clarify whether rising HK2 or glycolytic signatures herald the development of resistance. At the therapeutic level, rational combinations of sorafenib with glycolysis inhibitors, HIF pathway modulators or agents targeting downstream metabolic nodes could be tested, ideally in patient subsets stratified by hypoxia-related scores. By integrating spatial, metabolic and clinical data, it may become possible to distinguish patients whose resistance is predominantly driven by angiogenesis from those in whom tumor cell-intrinsic metabolic adaptation, such as that mediated by HK2, plays a larger role.

Conclusions

This study shows that in hepatocellular carcinoma, a hypoxia-enriched tumor subset engages a HIF1A-HK2 axis to enhance glycolytic metabolism and confer sorafenib tolerance through a predominantly tumor cell-intrinsic, rather than angiogenesis-dependent, mechanism.

Abbreviations

2-DG
2-deoxy-D-glucose
CCK-8
Cell Counting Kit-8
$CoCl_2$
Cobalt Chloride
Co-IP
Co-immunoprecipitation
DEGs
Differentially Expressed Genes
DMEM
Dulbecco’s Modified Eagle’s Medium
ECAR
Extracellular Acidification Rate
FBS
Fetal Bovine Serum
GAPDH
Glyceraldehyde-3-phosphate Dehydrogenase
GSEA
Gene Set Enrichment Analysis
GSVA
Gene Set Variation Analysis
HCC
Hepatocellular Carcinoma
HIF1A
Hypoxia-inducible Factor 1α
HK2
Hexokinase 2
HRE
Hypoxia Response Element
HUVECs
Human Umbilical Vein Endothelial Cells
IC_{50}
Half-maximal Inhibitory Concentration

LASSO
Least Absolute Shrinkage and Selection Operator
OS
Overall Survival
PCA
Principal Component Analysis
PVDF
Polyvinylidene Fluoride
RIPA
Radioimmunoprecipitation Assay
ROC
Receiver Operating Characteristic
scRNA-seq
Single-cell RNA Sequencing
SDS-PAGE
Sodium Dodecyl Sulfate-Polyacrylamide Gel Electrophoresis
siRNA
Small Interfering RNA
STR
Short Tandem Repeat
TCGA
The Cancer Genome Atlas
TME
Tumor Microenvironment
UMAP
Uniform Manifold Approximation and Projection
VEGF
Vascular Endothelial Growth Factor

Declarations

Ethics approval and consent to participate

Not applicable.

Consent for publication

Not Applicable.

Availability of data and materials

The datasets analysed in the current study are publicly available in the Gene Expression Omnibus (GEO) repository (https://www.ncbi.nlm.nih.gov/geo/) and TCGA databases (https://www.cancer.gov/ccg/research/genome-sequencing/tcga). The accession numbers for the GEO datasets is GSE149614.

Competing Interests

The authors declare no conflict of interest.

Funding

This work was supported by the Jinhua Science and Technology Plan Project (Social Development Project) (Grant Nos. 2023-3-097, 2024-3-043, and 2025-4-064) and the Special Fund for Basic Research of Jinhua Central Hospital (Grant Nos. JY2023-5-02 and JY2023-6-07).

Author contributions

Haijun Chen, Lujian Zhu and Xiaobo Wang contributed to the study design and manuscript writing. Junmei Lin and Hongjun Hua performed the data analysis. Experimental validation was performed by Xuxing Ye. Chao Yang assisted in the revision. All authors contributed to the writing of the manuscript and approved the version of the study as submitted.

Acknowledgments

We acknowledge TCGA and GEO database for providing their platforms and contributors for uploading their meaningful datasets.

References

1. An L, Li Z (2025) Molecular network of metabolic reprogramming and precision diagnosis and treatment of hepatocellular carcinoma. Biomark Res 13:124. https://doi.org/10.1186/s40364-025-00844-5
2. Bao MH, Wong CC (2021) Hypoxia, Metabolic Reprogramming, and Drug Resistance in Liver Cancer. Cells 10. https://doi.org/10.3390/cells10071715
3. Bray F, Laversanne M, Sung H, Ferlay J, Siegel RL, Soerjomataram I, Jemal A (2024) Global cancer statistics 2022: GLOBOCAN estimates of incidence and mortality worldwide for 36 cancers in 185 countries. CA Cancer J Clin 74:229–263. https://doi.org/10.3322/caac.21834
4. Caltana L, Merelli A, Lazarowski A, Brusco A (2009) Neuronal and glial alterations due to focal cortical hypoxia induced by direct cobalt chloride (CoCl2) brain injection. Neurotox Res 15:348–358. https://doi.org/10.1007/s12640-009-9038-9
5. Cao L, Wang M, Dong Y et al (2020) Circular RNA circRNF20 promotes breast cancer tumorigenesis and Warburg effect through miR-487a/HIF-1α/HK2. Cell Death Dis 11:145.

https://doi.org/10.1038/s41419-020-2336-0

6. Do MH, Shi W, Ji L et al (2023) Reprogramming tumor-associated macrophages to outcompete endovascular endothelial progenitor cells and suppress tumor neoangiogenesis. Immunity 56:2555–2569e2555. https://doi.org/10.1016/j.immuni.2023.10.010
7. Ferrer CM, Lynch TP, Sodi VL et al (2014) O-GlcNAcylation regulates cancer metabolism and survival stress signaling via regulation of the HIF-1 pathway. Mol Cell 54:820–831. https://doi.org/10.1016/j.molcel.2014.04.026
8. Garcia SN, Guedes RC, Marques MM (2019) Unlocking the Potential of HK2 in Cancer Metabolism and Therapeutics. Curr Med Chem 26:7285–7322. https://doi.org/10.2174/0929867326666181213092652
9. Hänzelmann S, Castelo R, Guinney J (2013) GSVA: gene set variation analysis for microarray and RNA-seq data. BMC Bioinformatics 14:7. https://doi.org/10.1186/1471-2105-14-7
10. Ho DW, Tsui YM, Chan LK et al (2021) Single-cell RNA sequencing shows the immunosuppressive landscape and tumor heterogeneity of HBV-associated hepatocellular carcinoma. Nat Commun 12:3684. https://doi.org/10.1038/s41467-021-24010-1
11. Jiang X, Zhang W, Li L, Xie S (2021) Integrated Transcriptomic Analysis Revealed Hub Genes and Pathways Involved in Sorafenib Resistance in Hepatocellular Carcinoma. Pathol Oncol Res 27:1609985. https://doi.org/10.3389/pore.2021.1609985
12. Jin P, Jiang J, Zhou L, Huang Z, Nice EC, Huang C, Fu L (2022) Mitochondrial adaptation in cancer drug resistance: prevalence, mechanisms, and management. J Hematol Oncol 15:97. https://doi.org/10.1186/s13045-022-01313-4
13. Jin S, Guerrero-Juarez CF, Zhang L et al (2021) Inference and analysis of cell-cell communication using CellChat. Nat Commun 12:1088. https://doi.org/10.1038/s41467-021-21246-9
14. Ladd AD, Duarte S, Sahin I, Zarrinpar A (2024) Mechanisms of drug resistance in HCC. Hepatology 79:926–940. https://doi.org/10.1097/hep.0000000000000237
15. Li M, Zhang X, Wang M et al (2022) Activation of Piezo1 contributes to matrix stiffness-induced angiogenesis in hepatocellular carcinoma. Cancer Commun (Lond) 42:1162–1184. https://doi.org/10.1002/cac2.12364
16. Li Y, Huan C, Sun H et al (2025) Spatial Transcriptomics and snRNA-seq Expose CAF Niches Orchestrating Dual Stromal-Immune Barriers in Hepatocellular Carcinoma. Adv Sci (Weinh) 12:e14661. https://doi.org/10.1002/advs.202514661
17. Lin Y, Zhang F, Guo W et al (2025) Hyperbaric oxygen targets RCN1 to modulate ER-mitochondria crosstalk and ameliorate sorafenib resistance in hepatocellular carcinoma. Drug Resist Updat 85:101342. https://doi.org/10.1016/j.drup.2025.101342
18. Liu S, Zhang X, Wang W et al (2024) Metabolic reprogramming and therapeutic resistance in primary and metastatic breast cancer. Mol Cancer 23:261. https://doi.org/10.1186/s12943-024-02165-x
19. Lu Y, Yang A, Quan C et al (2022) A single-cell atlas of the multicellular ecosystem of primary and metastatic hepatocellular carcinoma. Nat Commun 13:4594. https://doi.org/10.1038/s41467-022-

32283-3

20. Maeser D, Gruener RF, Huang RS (2021) oncoPredict: an R package for predicting in vivo or cancer patient drug response and biomarkers from cell line screening data. https://doi.org/10.1093/bib/bbab260. Brief Bioinform 22
21. Newman AM, Liu CL, Green MR et al (2015) Robust enumeration of cell subsets from tissue expression profiles. Nat Methods 12:453–457. https://doi.org/10.1038/nmeth.3337
22. Peng C, Ni W, Liu Q, Hu G, Zheng W (2025) A comprehensive benchmarking of the AlphaFold3 for predicting biomacromolecules and their interactions. Brief Bioinform 26. https://doi.org/10.1093/bib/bbaf616
23. Ritchie ME, Phipson B, Wu D, Hu Y, Law CW, Shi W, Smyth GK (2015) limma powers differential expression analyses for RNA-sequencing and microarray studies. Nucleic Acids Res 43:e47. https://doi.org/10.1093/nar/gkv007
24. Sangro B, Argemi J, Ronot M et al (2025) EASL Clinical Practice Guidelines on the management of hepatocellular carcinoma. J Hepatol 82:315–374. https://doi.org/10.1016/j.jhep.2024.08.028
25. Satija R, Farrell JA, Gennert D, Schier AF, Regev A (2015) Spatial reconstruction of single-cell gene expression data. Nat Biotechnol 33:495–502. https://doi.org/10.1038/nbt.3192
26. Semenza GL (2002) HIF-1 and tumor progression: pathophysiology and therapeutics. Trends Mol Med 8:S62–67. https://doi.org/10.1016/s1471-4914(02)02317-1
27. Shan Q, Yin L, Zhan Q et al (2024) The p-MYH9/USP22/HIF-1α axis promotes lenvatinib resistance and cancer stemness in hepatocellular carcinoma. Signal Transduct Target Ther 9:249. https://doi.org/10.1038/s41392-024-01963-5
28. Sun H, Li XB, Meng Y, Fan L, Li M, Fang J (2013) TRAF6 upregulates expression of HIF-1α and promotes tumor angiogenesis. Cancer Res 73:4950–4959. https://doi.org/10.1158/0008-5472.Can-13-0370
29. Tang L, Zeng J, Geng P et al (2018) Global Metabolic Profiling Identifies a Pivotal Role of Proline and Hydroxyproline Metabolism in Supporting Hypoxic Response in Hepatocellular Carcinoma. Clin Cancer Res 24:474–485. https://doi.org/10.1158/1078-0432.Ccr-17-1707
30. Tang W, Chen Z, Zhang W et al (2020) The mechanisms of sorafenib resistance in hepatocellular carcinoma: theoretical basis and therapeutic aspects. Signal Transduct Target Ther 5:87. https://doi.org/10.1038/s41392-020-0187-x
31. Wang J, Huang Q, Hu X et al (2022) Disrupting Circadian Rhythm via the PER1-HK2 Axis Reverses Trastuzumab Resistance in Gastric Cancer. Cancer Res 82:1503–1517. https://doi.org/10.1158/0008-5472.Can-21-1820
32. Wang Y, Zhang J, Shi H et al (2024) M2 Tumor-Associated Macrophages-Derived Exosomal MALAT1 Promotes Glycolysis and Gastric Cancer Progression. Adv Sci (Weinh) 11:e2309298. https://doi.org/10.1002/advs.202309298
33. Wang Z, Zhang C, Yin J, Li N (2025) Conversion therapy with TACE, TKIs, and ICIs for unresectable BCLC stage B and C hepatocellular carcinoma. Front Immunol 16:1451965.

https://doi.org/10.3389/fimmu.2025.1451965

34. Yan J, Chen D, Ye Z et al (2024) Molecular mechanisms and therapeutic significance of Tryptophan Metabolism and signaling in cancer. Mol Cancer 23:241. https://doi.org/10.1186/s12943-024-02164-y
35. Yang WH, Qiu Y, Stamatatos O, Janowitz T, Lukey MJ (2021) Enhancing the Efficacy of Glutamine Metabolism Inhibitors in Cancer Therapy. Trends Cancer 7:790–804. https://doi.org/10.1016/j.trecan.2021.04.003
36. Yang Y, Ni Q, Li H et al (2025) Genomic and the tumor microenvironment heterogeneity in multifocal hepatocellular carcinoma. Hepatology 82:582–598. https://doi.org/10.1097/hep.0000000000001191
37. Zeng F, Zhang Y, Han X, Zeng M, Gao Y, Weng J (2021) Employing hypoxia characterization to predict tumour immune microenvironment, treatment sensitivity and prognosis in hepatocellular carcinoma. Comput Struct Biotechnol J 19:2775–2789. https://doi.org/10.1016/j.csbj.2021.03.033
38. Zhan Y, Sun D, Gao J et al (2025) Single-cell transcriptomics reveals intratumor heterogeneity and the potential roles of cancer stem cells and myCAFs in colorectal cancer liver metastasis and recurrence. Cancer Lett 612:217452. https://doi.org/10.1016/j.canlet.2025.217452
39. Zhang B, Tang B, Gao J, Li J, Kong L, Qin L (2020) A hypoxia-related signature for clinically predicting diagnosis, prognosis and immune microenvironment of hepatocellular carcinoma patients. J Transl Med 18:342. https://doi.org/10.1186/s12967-020-02492-9
40. Zhang Q, Qiao L, Liao J, Liu Q, Liu P, Liu L (2021) A novel hypoxia gene signature indicates prognosis and immune microenvironments characters in patients with hepatocellular carcinoma. J Cell Mol Med 25:3772–3784. https://doi.org/10.1111/jcmm.16249
41. Zhu L, Ao L, Guo Z et al (2024) Recombinant canstatin inhibits the progression of hepatocellular carcinoma by repressing the HIF-1α/VEGF signaling pathway. Biomed Pharmacother 179:117423. https://doi.org/10.1016/j.biopha.2024.117423

Figures

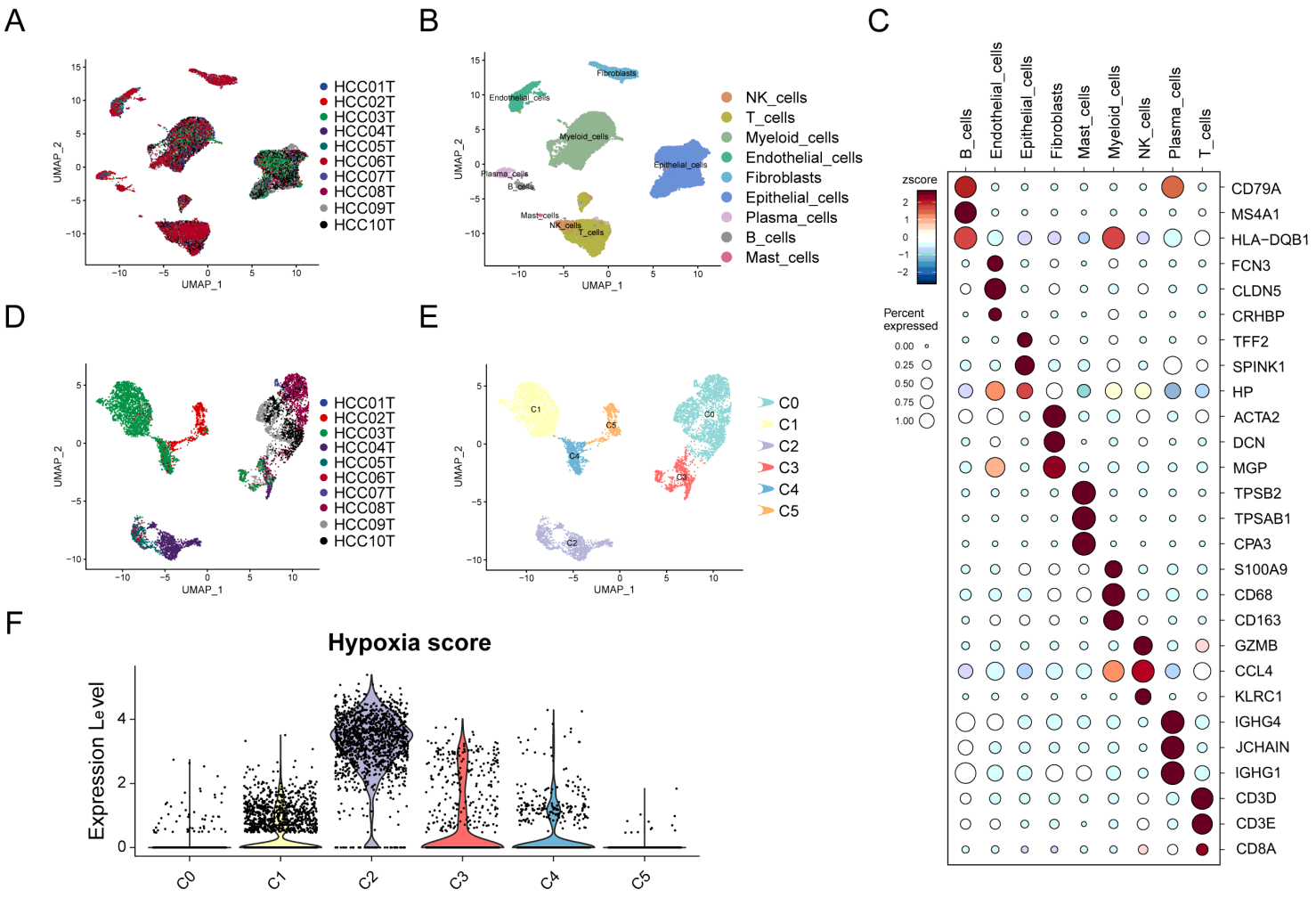


Figure 1

Single-cell transcriptome profiling and hypoxia-related tumor cluster identification in HCC. (A). UMAP displaying cell distribution across ten HCC samples. (B). Annotated UMAP showing major cell lineages including epithelial, endothelial, myeloid, fibroblast, plasma and immune subsets. (C). Dot-plot of representative markers for cell-type assignment. (D). Sample-coloured UMAP for batch visualization. (E). Subclustering of epithelial/tumor compartment into five subgroups (C0-C5). (F). Violin plot of hypoxia score distribution among tumor subclusters.

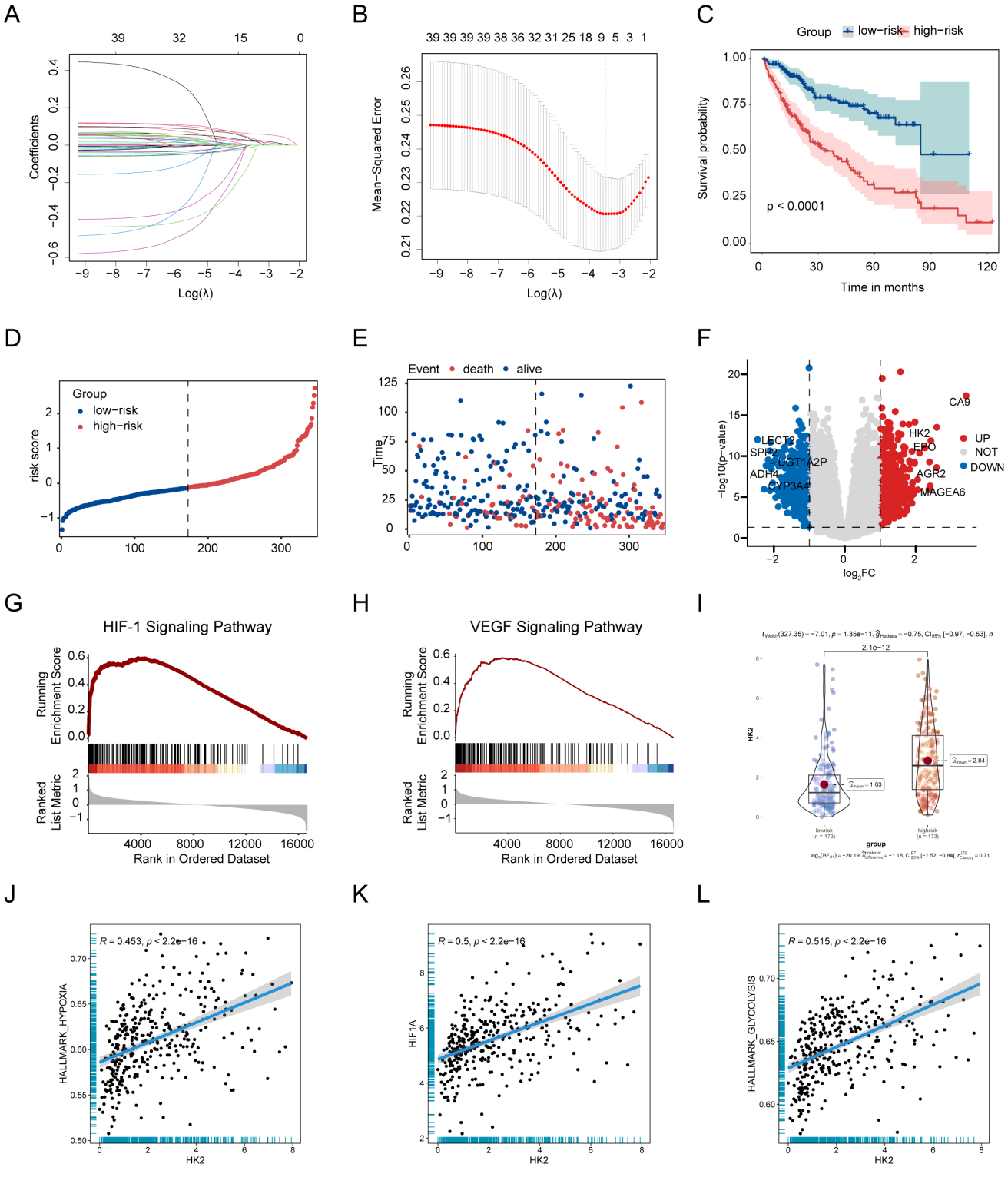


Figure 2

Construction of a hypoxia-related prognostic model in HCC. (A). LASSO coefficient trace for hypoxia-linked genes across penalty values. (B). Ten-fold cross-validation curve of LASSO-Cox model with optimal λ indicated. (C). Kaplan-Meier curves comparing overall survival in two risk groups. (D). Rank-ordered risk score distribution and median cutoff assignment. (E). Survival status plot aligned with patient risk score. (F). Volcano plot showing differential gene expression between risk groups. (G-H).

GSEA plots for HIF-1 and VEGF pathways. (I). Violin plots of pathway scores in two risk strata. (J-L). Correlation plots among HK2, hypoxia-index variables and glycolysis metric.

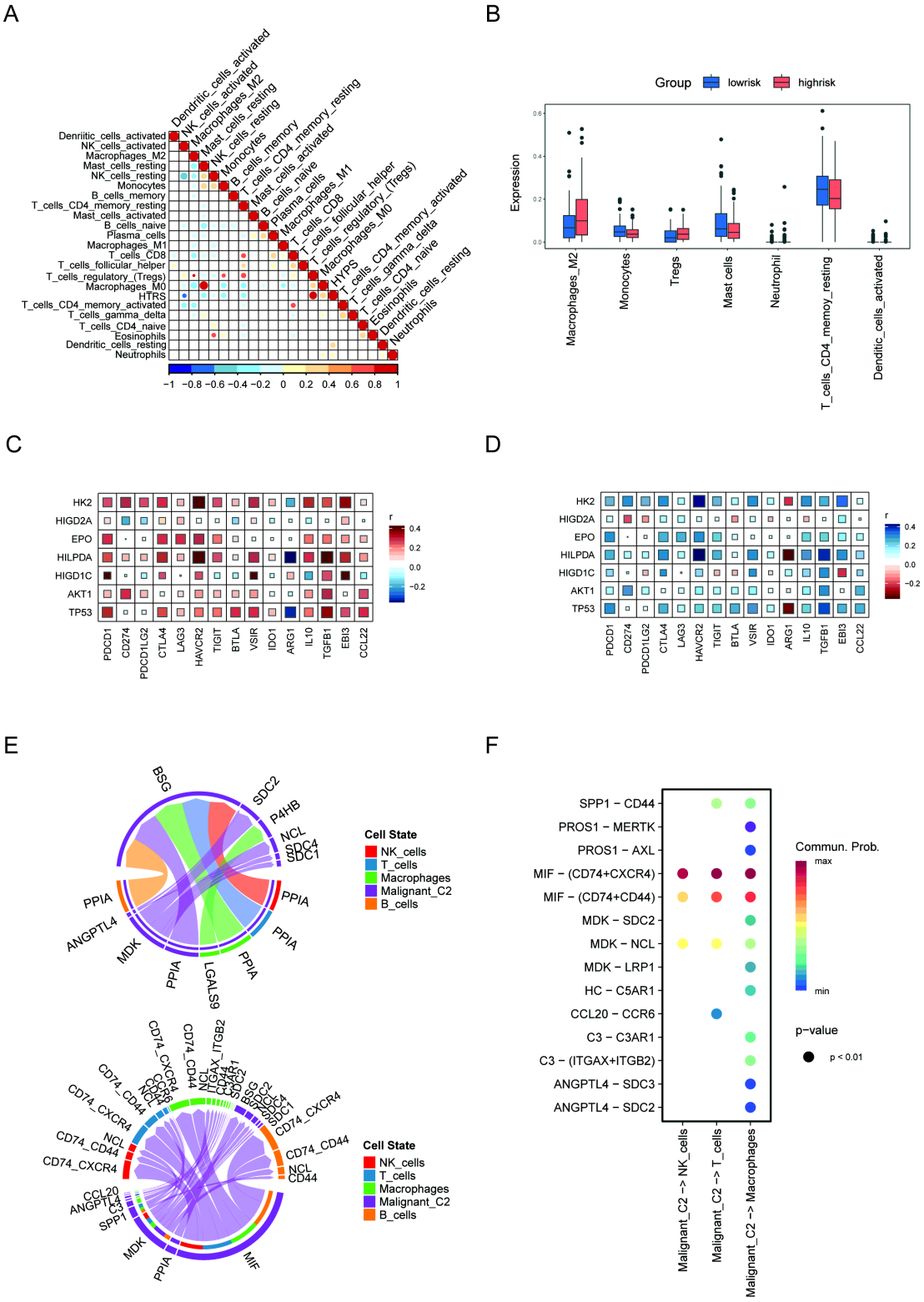


Figure 3

Immune infiltration and signalling features associated with hypoxia-risk groups.(A). Correlation matrix of infiltrating immune subsets. (B). Boxplot of immune-cell fractions across risk groups. (C-D). Heatmaps showing correlation between HK2-related hypoxia-genes and immune-regulatory genes under two

scoring systems. (E). Circos visualization of ligand-receptor interactions among tumor and immune subsets. (F). Dot matrix of the most probable signalling interactions with communication probability ranking.

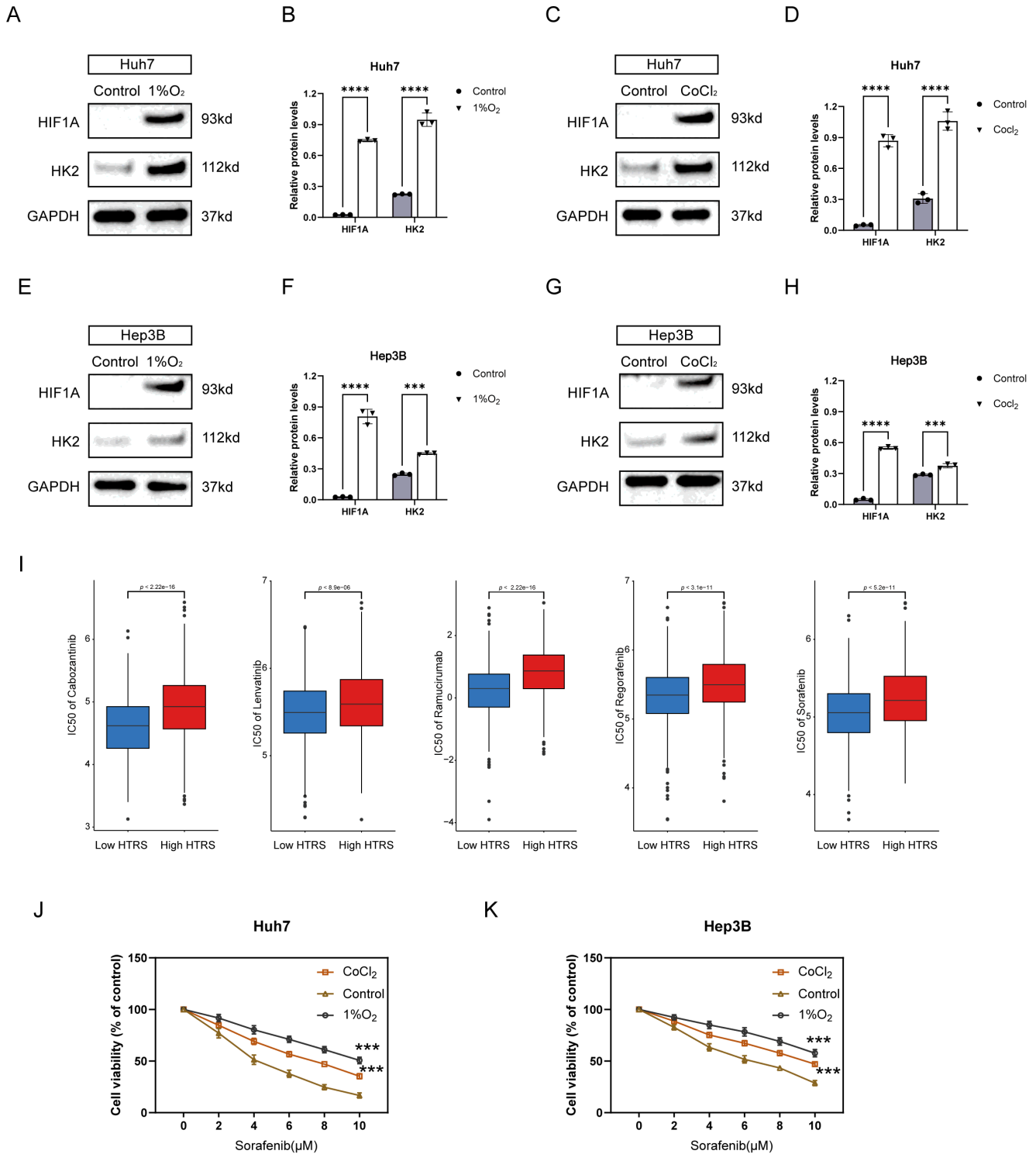


Figure 4

Hypoxia-induced protein expression and drug response assessment in Huh7 and Hep3B cells.(A). Western blot bands of HIF1A, HK2 and GAPDH in Huh7 under normoxia and 1% O_2. (B). Relative

quantification of HIF1A and HK2 protein levels in Huh7 corresponding to panel (A). (C). Western blot detection of HIF1A, HK2 and GAPDH in Huh7 following $CoCl_2$ treatment. (D). Quantified expression of HIF1A and HK2 in Huh7 corresponding to panel (C). (E). Western blot visualization of HIF1A, HK2 and GAPDH in Hep3B under normoxia and 1% O_2. (F). Quantified protein expression in Hep3B corresponding to panel (E). (G). Western blot results of HIF1A, HK2 and GAPDH in Hep3B treated with $CoCl_2$ or control. (H). Quantification of protein bands corresponding to panel (G). (I). Boxplots displaying IC50 distribution of Cabozantinib, Lenvatinib, Ramucirumab, Regorafenib and Sorafenib between low- and high-risk groups. (J-K). Viability curves of Huh7 (J) and Hep3B (K) treated with graded sorafenib concentrations under normoxia, $CoCl_2$ or 1% O_2.

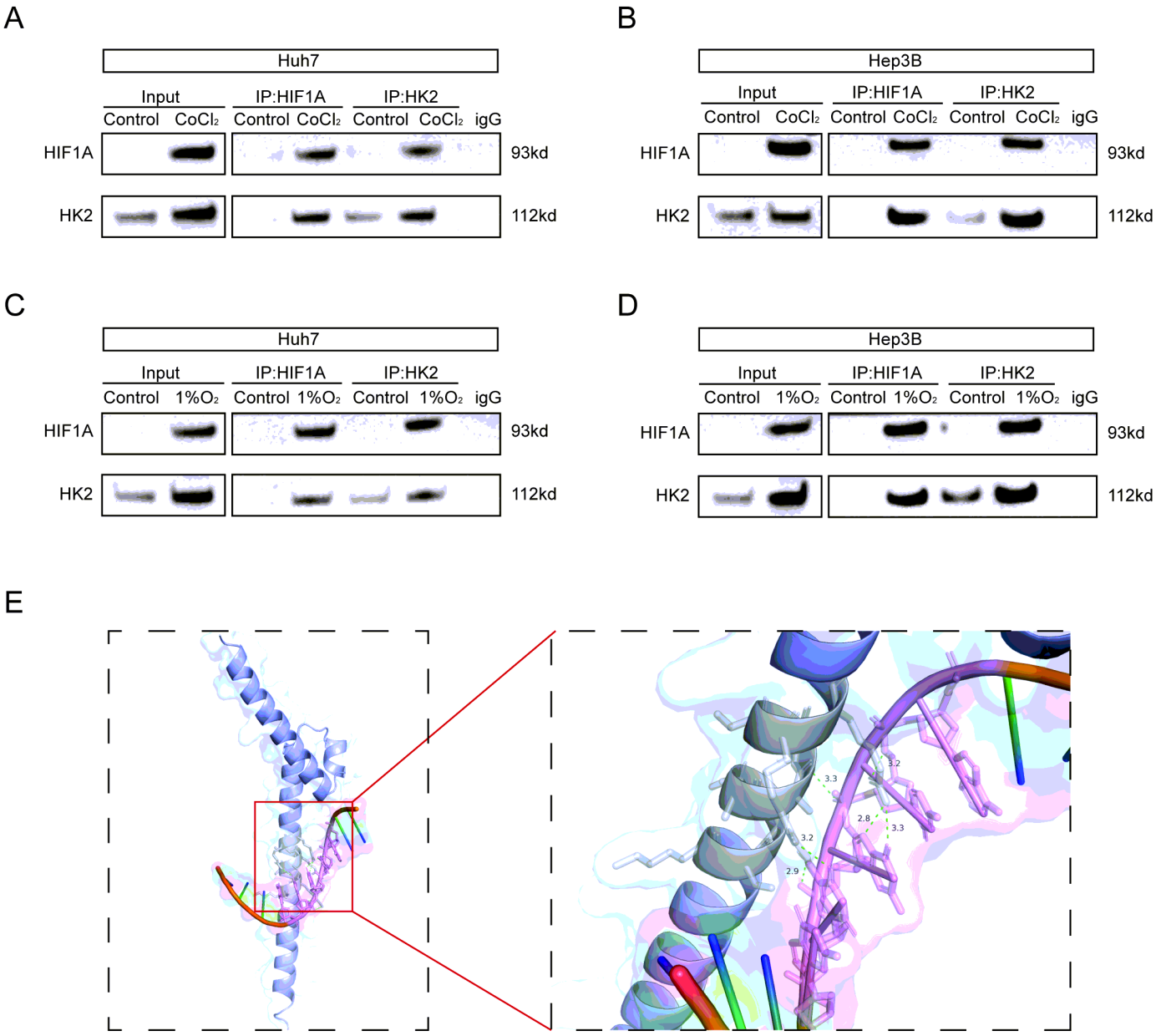


Figure 5

HIF1A-HK2 interaction verified by co-immunoprecipitation and structural docking.(A-D). Co-IP of HIF1A and HK2 in Huh7 and Hep3B cells under normoxia, $CoCl_2$ or 1% O_2 conditions using anti-HIF1A or anti-HK2 antibodies. (E). AlphaFold3-generated structural model of HIF1A bound to an HK2 promoter fragment containing HRE; HK2-DNA is displayed as colored sticks with the HRE highlighted in magenta, HIF1A is shown as a light-blue cartoon with the DNA-binding region in gray, and predicted hydrogen-bond contacts are marked with green dashed lines.

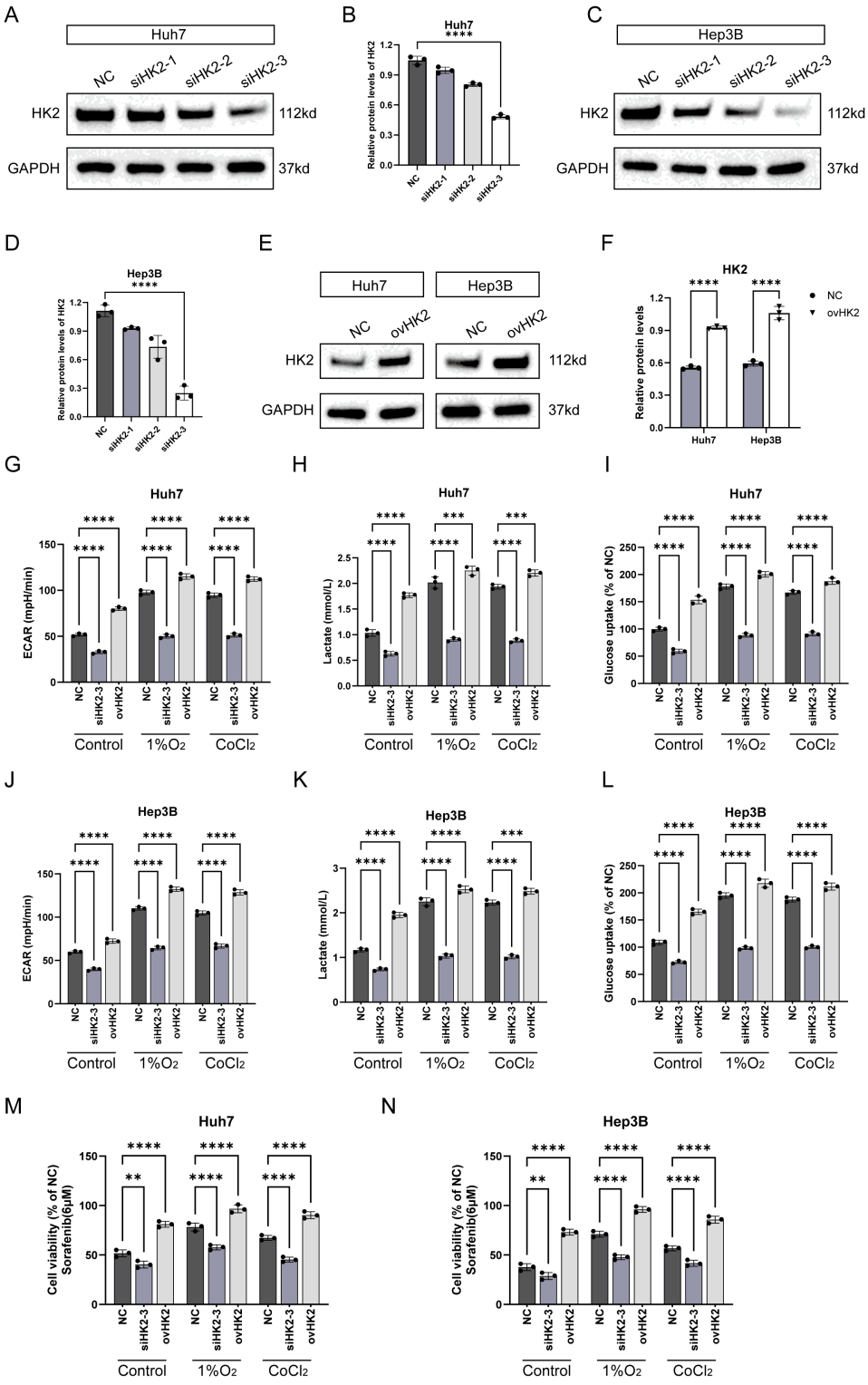


Figure 6

Functional assessment of HK2 knockdown and overexpression in hepatocellular carcinoma cells. (A-D). Western blot and densitometric quantification of HK2 expression in Huh7 and Hep3B following siHK2 interference. (E-F). Western blot and quantification of HK2 levels in Huh7 and Hep3B with HK2 overexpression. (G-I). ECAR, lactate production and glucose uptake of Huh7 under Control, 1% O_2 or $CoCl_2$ conditions with HK2 knockdown or overexpression. (J-L). ECAR, lactate production and glucose uptake of Hep3B under Control, 1% O_2 or $CoCl_2$ conditions with HK2 knockdown or overexpression. (M-N). Cell viability of Huh7 and Hep3B treated with sorafenib (6 μM) under Control, 1% O_2 or $CoCl_2$ conditions across HK2-NC, siHK2 and ovHK2 groups.

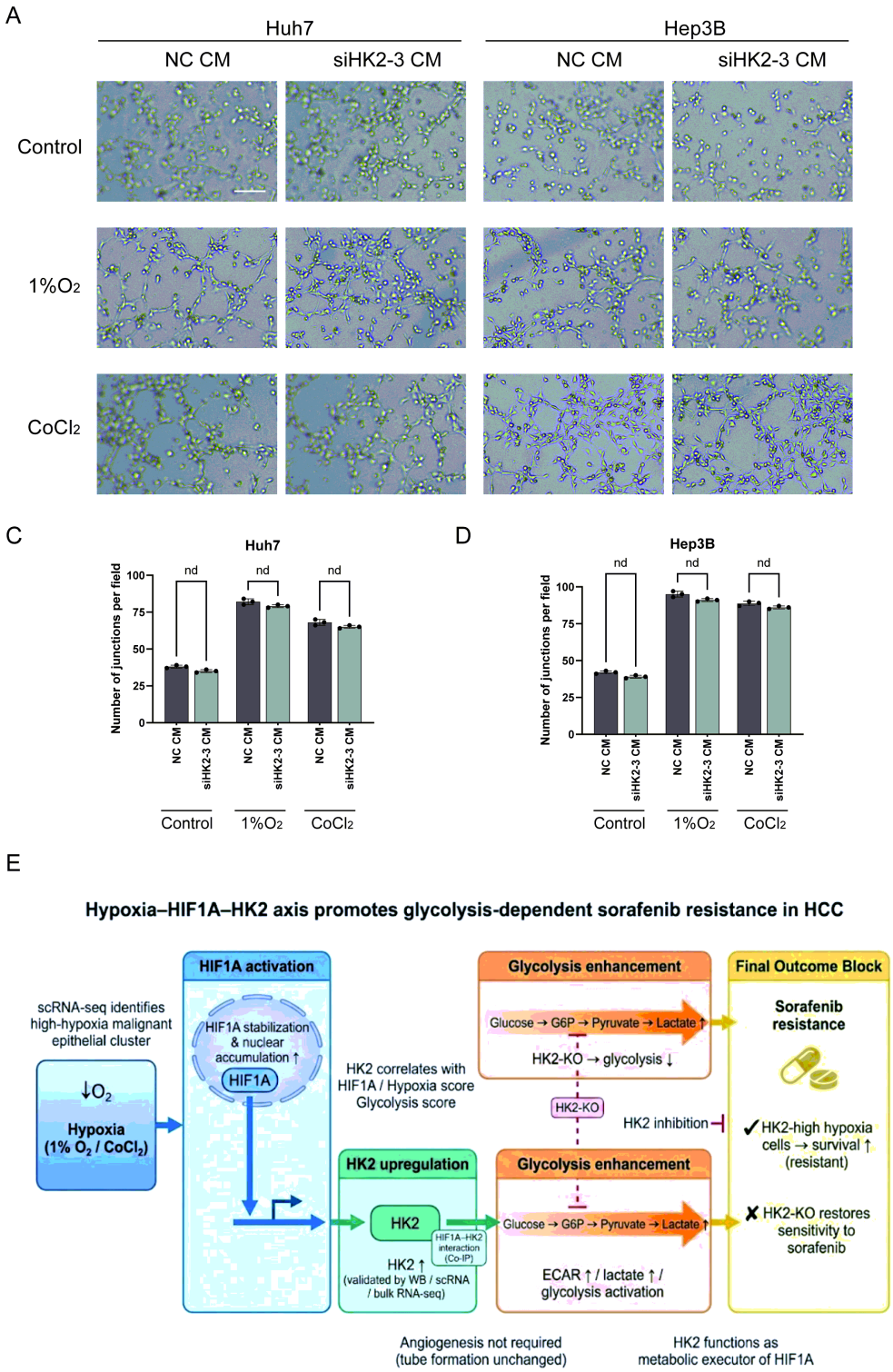


Figure 7

Tube formation assay and schematic illustration of the hypoxia-HIF1A-HK2 axis.(A-B). Representative HUVEC tube formation images using conditioned medium (CM) from Huh7 or Hep3B cells with HK2 knockdown or control under normoxia, 1% O_2, or $CoCl_2$. (C-D). Quantification of junction number per field in the indicated groups. (E). Working model summarizing the hypoxia-HIF1A-HK2 regulatory axis: hypoxia

stabilizes HIF1A, elevates HK2 expression, enhances glycolytic flux and sustains sorafenib survival advantage without altering tube-forming phenotype.